ORIGINAL ARTICLE

A perspective review: Technical study of combining phase contrast magnetic resonance imaging and computational fluid dynamics for blood flow on carotid bifurcation artery

Mohd Azrul Hisham Mohd Adib[1], Lim Sheh Hong[1], Mohd Shafie Abdullah[2], Radhiana Hassan[3], Azian Abd Aziz[3], and Shigeo Wada[4]

[1] Medical Engineering & Health Intervention Team (MedEHiT), Department of Mechanical Engineering, College of Engineering, Universiti Malaysia Pahang, 26600 Pekan, Pahang, Malaysia. Phone: +6094246246; Fax: +6094242202

[2] Department of Radiology, School of Medical Sciences, Health Campus, Universiti Sains Malaysia, 16150 Kubang Kerian, Kelantan, Malaysia

[3] Department of Radiology, Kulliyyah of Medicine, International Islamic University Malaysia, 25200 Kuantan, Pahang, Malaysia

[4] Graduate School of Engineering Science, Osaka University, Machikaneyama- Chou 1-3, Toyonaka, Osaka 560-8531, Japan

ABSTRACT – Nowadays, the knowledge of precise blood flow patterns in human blood vessels, especially focusing on Carotid Bifurcations Artery (CBA) area by using computational and modern techniques are very important to develop our understanding regarding to human diseases for both essential research and clinical treatment. This paper tends to discuss the progress regarding to the integration between Phase Contrast Magnetic Resonance Imaging (PC-MRI) and Computational Fluid Dynamics (CFD), specifically to the human diseases. We technically define the model geometry reconstruction, review both PC-MRI and CFD methods to create mesh models, obtain boundary conditions, define the governing equations in CFD, define the material properties, and assumptions used in running the CFD simulations. Detailed information on PC-MRI and CFD is provided in tables, such as the MRI setup, software used, CFD model setup, measurement parameter, and summary of the result contribution from each reviewed article. Numerous fusions between PC-MRI and CFD are specified by summarizing the investigation carried out by significant group's research, reviewing the important outcomes, and discussing the techniques, drawbacks and possibilities for further study. We hope that this perspective analysis will encourage a fusion of PC-MRI and CFD research contributing to continuous advancement of human health with close cooperation and collaboration among clinicians and engineers.

INTRODUCTION

Nowadays, Computational Fluid Dynamics (CFD) studies are improving significantly. With initially verifying the result value of military purposes [1], CFD has been acknowledged as the most important study to the automobile industry, chemical engineering, machinery, and also for aviation. Nevertheless, CFD is applied widely in the biomechanical and biomedical engineering fields in the current trend [2]. The simulation of airflow distribution in the bronchial studies [3] and the velocity flow simulation in cardiovascular circulation [4, 5] are the examples of the biomechanical engineering field in which CFD studies are much needed for future interventions. In cardiovascular circulation, CFD studies are very dedicated to manipulating variables, especially in fluid velocity profile and deriving some equations from parameters such as force (F), pressure (P) [6], and wall shear stress (WSS) [7]. Phase Contrast Magnetic Resonance Imaging (PC-MRI) has been recognized as the reflection instruments in artificial structure research [8] and the method is presented as three-dimensional (3D) PC-MRI in the investigation. The integration between PC-MRI and CFD has already shown in the research conducted by Wood et al. [9] with a detailed explanation for the blood flow inside the aorta of heart and also simulation on the corrected way of lower or higher WSS where it correlated to areas of arteriosclerosis problems. Several research groups did the same observation but practically focus on Carotid Bifurcation Artery (CBA) [10–17]. From the previous studies [18–21], the authors have investigated the abdominal bifurcation. Time is very compulsory when we use the MRI measurement and until now, there is no journal reporting the interest that can be gifted always [22]. The CFD can compute the gaps between the calculated data and actual PC-MRI measurements, however, the acceptable integration between both PC-MRI and CFD simulation velocity data is required. Too many techniques or setups for conducting simulation have been found from the previous studies but there is less or no research concerning the integration between PC-MRI measurements and CFD simulation, typically on velocity flow field and WSS distribution. This perspective review tends to describe the technical aspects of model geometry reconstruction, review on both CFD and PC-MRI methods, compare the mesh models, obtain boundary conditions, define the governing equations in CFD, define the material properties, and assumptions used in running the CFD simulations.

PC-MRI PERSPECTIVE

Presently, the best collective biomedical imaging procedures which cast off to restructure Carotid Bifurcation Artery (CBA) model geometry are Megnetic Resonance Imaging (MRI) and Computed Tomography (CT) scan. The CT scan is an effective tool for generating X-ray images by classifying human body parts. These images with high contrast resolution allow whole human body to be examined through a small change in the resolution of the distinction. However, the MRI uses strong magnetic field instead of X-ray radiation which provide clearer image data on the vacular parts as compared to the CT scan. For the determination of CBA imaging, the Phase Contrast Magnetic Resonance Imaging (PC-MRI) result is mostly a very good prediction since the blood itself can be substituted for a contrast terminal. Besides, the PC-MRI may use to measure blood flow rates with time-varying and offer the required flow velocity boundary conditions at both artery inlets and outlets which are unavailable in the CT scan [23].

The model geometry reconstruction usually involves two main stages after image acquisition: image segmentation and surface modelling [24,25]. Generally, the image-based reconstruction methods are based on two-dimensional (2D) segmentation [26, 27]. The threshold of image intensity is used to automatically detect the area of images that can be measured in the investigated model. These techniques can be performed with modifications where it depends on the software used either with more or less automation in the detection of data resolution and also the resolution of the medical image data [25].

PC-MRI Geometry Detection

In the medical perspective, the blood and vessel wall are the parameters to be well-known in PC-MRI. Research has been ongoing for years and the consistency of the measurement result obtained from PC-MRI is very significant [28]. Numerous segmentation methods available nowadays are mainly based on artificial intelligence (AI) recognition and mathematical algorithm or modelling [29]. However, there is a consequence of error on the velocity vector data measured in a straight tube geometry with the use of mathematical modelling in segmenting image data as reported by Moore et al. [30]. Table 1 shows the synopsis of voxel size achievement components in the formerly observed integration between CFD and PC-MRI. In this investigation into the detection of vessel model geometry using PC-MRI, there are three basic problems detected which are the technique of smoothing process, the chosen optimal voxel size, and the noise at the PC-MRI measurements.

Table 1. Synopsis of voxel size achievement components on the integration between PC-MRI and CFD [31]

Author	Aim of the study	b (mm)	a (mm)	△t (ms)
Thomas et al. [16]	Carotid bifurcation	0.313	2	-
Weston et al. [32]	U tube	0.78	2	40
Long et al. [19]	Abdominal bifurcation	1.25	1.5	-
Xu et al. [21]	Abdominal bifurcation	0.94	1.5	-
Long et al. [13]	Carotid bifurcation	0.47	5	NA
Long et al.[18]	Abdominal bifurcation	1.09	1.5	-
Botnar et al. [33]	Carotid bifurcation	0.5	4	25
Ladak et al. [14]	Carotid bifurcation	0.31	2	NA
Zhao et al. [12]	Carotid bifurcation	0.47	1.5	-

△t is time varying flow between 2 acquisitions, **"a"** refers to slice thickness, **"b"** refers to pixel size

Vessel Geometry Segmentation and Assessment to Inflow and Outflow with MRI

The user must define a start and an endpoint on the vessel to be analyzed in the 3D data space. The vessel segment is then automatically detected based on the level set method (threshold). After these segmentation processes and 3D reconstruction of the vessel, the cross-sections along the vessel are calculated. Once the geometry of the vessel is recognized, the inflow and outflow distributions are compulsory for the assessment of velocity profiles and WSS distributions. To reach the accurate inflow and outflow data, it is required to have a description of velocity profiles at specific positions. It is based on a standard MRI blood flow achievement yielding accurate and incorrect flow data distribution [22]. It is presumed that the parabolic flow velocity profiles in both straight tube and CBA models as shown in Figure 1 are the efficient models for blood flow in small diameter vessels with a relatively steady rate of flow. Details from the previous studies on the flow acquisition with PC-MRI setup are listed in Table 2 and Table 3 in the following section**.**
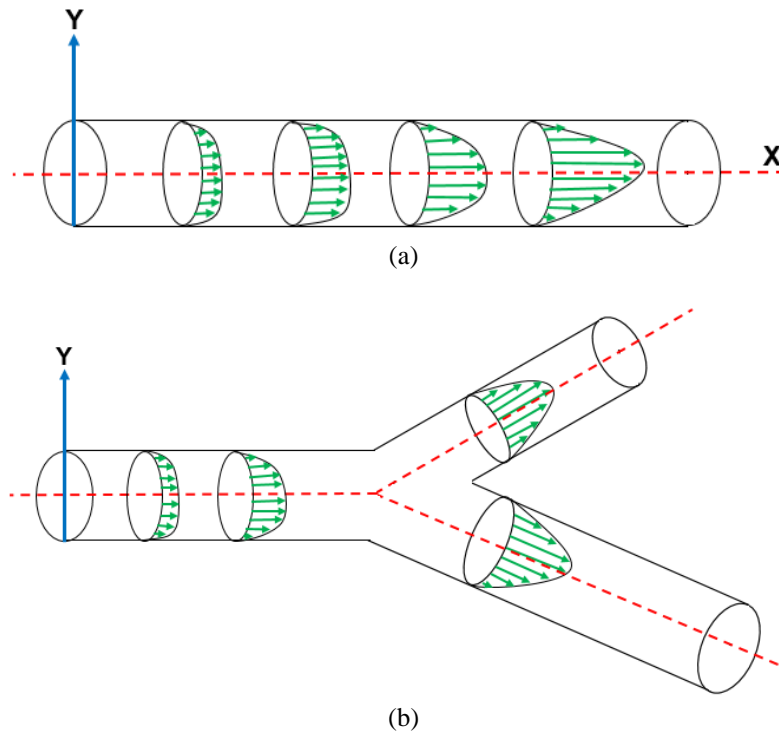
(a)

(b)

Figure 1. Development of steady blood flow through (a) Straight tube and (b) Carotid Bifurcation Artery (CBA) with parabolic flow velocity profiles [34, 35]

Table 2. The difference between inlet and outlet boundary condition type with PC-MRI integrated CFD [31]

Author	Target	Geometry	Inflow	Outflow
Thomas et al. [16]	Carotid bifurcation	By hand	MR	MR
Weston et al. [32]	U tube	Prescribe	Uniform pressure	MR
Long et al. [19]	Abdominal bifurcation	Snake	Mass	MR
Xu et al. [21]	Abdominal bifurcation	Snake	MR+Mass	MR
Long et al. [13]	Carotid bifurcation	Snake	MR+Mass	MR
Long et al. [18]	Abdominal bifurcation	Snake	MR+Mass	MR
Botnar et al. [33]	Carotid bifurcation	WLS	MR	NA
Ladak et al. [14]	Carotid bifurcation	Balloon	MR	MR
Zhao et al. [12]	Carotid bifurcation	Snake	Uniform pressure	Mass
Cebral et al. [17]	Carotid bifurcation	TDF	MR	MR

TDF: tubular deformable model, **WLS:** surface modeling using weighted least squares splines, **Mass:** mass preservation, **MR:** MRI velocity measurement, **Uniform pressure:** a uniform pressure distribution is set on the boundary, **Snake:** snake model, **Balloon:** balloon model, **NA:** not available

Mesh Generation based on a Segmented Vessel

The current method for mesh generation of a PC-MRI data set will be described particularly on a CBA. Each segmented vessel is stated as a load of cross-sections while the CBA is defined by three segmented vessel with each involving a load of cross-sections as shown in Figure 2(b). Figure 2(c) illustrates the locations where the PC-MRI velocity profiles are measured. To simulate the region between the measured inflow and outflow cross-sections, the segmented image is cut off at these positions as shown in Figure 2(c). The cross-sections of the model geometry segmented from PC-MRI were converted to rectangles with the same 3D distribution as the rectangles at the mesh surface. Lastly, the standard mesh was changed until it matched the segmented data set as shown in Figure 2(d) [36].
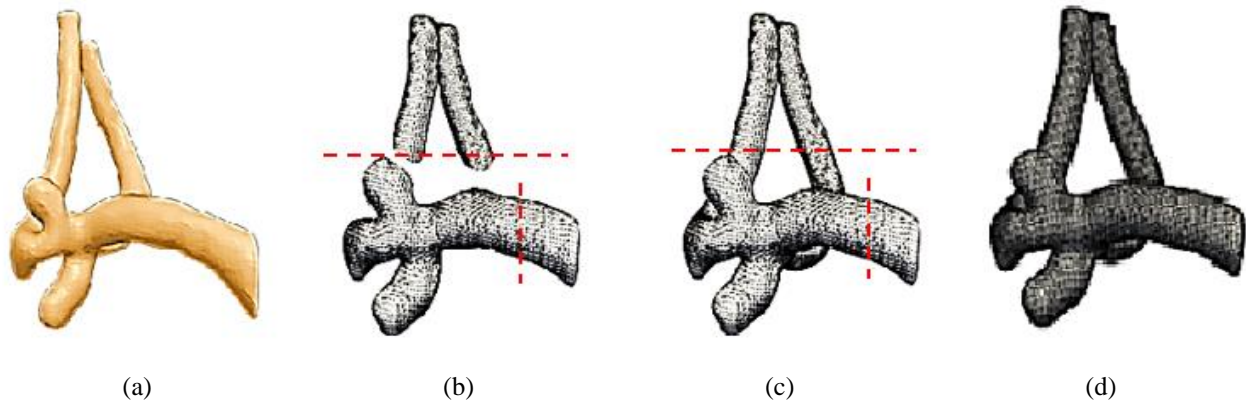
| (a) | (b) | (c) | (d) |

Figure 2. (a) PC-MRI image; (b) Segmented image; (c) Position of velocity and (d) Matched mesh

CFD PERSPECTIVE

CFD Geometry Setup

The first step of pretending blood flow (hemodynamics) is the creation of the CBAs model geometry structure in CFD. There have been numerous computational studies reporting the geometrical setup with a flow dynamic pattern in both steady flow and unsteady flow conditions [37–43]. Most of the studies claimed that there are difficulties in extracting model geometry measurements and velocity flow patterns. Some researchers also established the effect of arch curvature, the resulting velocity profiles and the configuration of the flow patterns in the investigated model geometries.

Mesh Generation Process

In producing a 3D model geometry through the discretization method of the CFD domain, we need to choose among structured (hexahedral) or unstructured (tetrahedral or polyhedral) mesh types. For curved branch or unrealistic CBA geometries, hexahedral mesh type is preferred. In the patient with aneurysms, the most collective method is to use unstructured mesh created by feasible meshing tools, however it requires a different resolution for spreading mesh independence through lower computational costs than structured meshes. Further improvements were also notified in additional studies and the weak orientation with the crucial flow direction and the high numerical diffusion error associated with unstructured meshes were recognized [44]. Hexahedral meshes have been known to provide greater accuracy but are typically more difficult to generate in complex geometries. Table 4 presents the mesh types used by a few authors' simulations. Besides, mesh improvement has been infrequently distinguished as the curcial factor by Prakash et al. [7] and the resolution of WSS is regularly needed to give more attention. The mesh generation of boundary layer methods can also be practiced to upsurge the mesh density close to the wall of arterial [45].

Material Properties for Human Blood

It is known that human blood is highly complex. Originally, the human blood is considered as a non-Newtonian fluid with relation to the shear rate factor, but it is regularly assumed as a Newtonian fluid in the CFD studies. Although some previous studies have initiated important modifications between the results from CFD analysis with and without non-Newtonian fluids [46–48], most authors claimed that the Newtonian approach is basically perfect in terms of approximation based on theories [49]. The key reason for not considering non-Newtonian feature of blood is due to the high shear rates at artery with large diameter, especially in transient flow environments, after slow or converse blood flow, which make the non-Newtonian properties to be illogical.

Mechanics of Blood Flow in Arteries using Governing Equation

Throughout the field of engineering, a set of partial differential equations (PDE) known as the Navier–Stokes equations can accurately describe the 3D fluid flows in a mathematical form. They are focusing on the law of motion (momentum equation), mass conservation (continuity equation), and energy conservation (equation of energy). Under the premises [34] of an incompressible, homogenous, and Newtonian fluid, the Navier–Stokes equations can be defined as:

$$\rho \frac{\partial u}{\partial t} + \rho (u.\nabla) u = -\nabla p + \mu \nabla^2 u \tag{1}$$

$$\nabla.u = 0 \tag{2}$$

where the main variables are the velocity vector, u = [u,v,w], and the pressure, p that varies in space x, y, z as well as time, t. By considering the variables, the non-Newtonian effect is possible if the above equations are correctly modified [34]. These PDEs have an empirical approach for certain basic cases [50, 51]. Nevertheless, the structure of Navier–Stokes equations by mathematical approaches should be clarified at flows containing complex geometries and boundary conditions. Finite Element Methods (FEM) and Finite Volume Methods (FVM) appear to be important for solving the governing equations. Many research groups have already established their CFD solvers to raise their exact difficulties faced. Meanwhile, CFD also uses iterative approaches to solve the governing equations (GE). Different investigators practice different procedures of GE but it is general to express some local and global flow parameters that would enter a steady-state in residuals that would decrease below the threshold value [34]. Arteries are represented as rigid-wall and the blood is expected to be a homogeneous incompressible Newtonian fluid [26, 35, 52, 53].

Observation to Previous Literature Study with Velocity Profile and Flow Rate as Boundary Condition

From our investigation, several researchers set the flow rate distributions and flow velocities into PC-MRI on the inlets and outlets models [9, 13, 18–21, 32, 33, 54]. As we know, the boundary conditions have numerous solutions such as the pressure distribution setup on inflow and outflow [9], a condition of mass conservation [19, 20], MRI velocity profile [13, 18, 21, 32], and the uniform velocity profile [32]. It is also found that a few research groups set the developed blood flow velocity profiles on the inlet area of lumens. Either using PC-MRI [14–17] or Doppler [12], the evaluated time-varying flow rates are considered. The expected errors in the CFD will be introduced when the privation of consistency in the flow measurements occurs. From Weston et al. [32], the authors used the measurement data from MRI and they found that a steady stage condition of flow rate achieved was about 16% higher than that from the CFD results. In other cases, they found about 15% of the mean flow rate from PC-MRI was high as compared to what CFD measured. So from the overall investigation on measuring the flow rate, there has no author successfully set the flow rate with the highest accuracy into MRI flow velocity data on every boundary condition. It is known that the correct flow rate is not essentially the prediction from the calculated flow velocity. From Long et al. [13], they claimed that the moderately large inconsistencies flow were always found between PC-MRI integrated CFD measurement data. Wood et al. [9] reported that the CFD analysis on a human descending aorta usually detected variances from the meantime of flows: 5000 mL/min and 3500 mL/min at the inlet and outlet, respectively [34]. These inconsistencies are certified to the measurement of the uncertainties effects at small outflow branches. About ± 28% of uncertainty was found from the CFD flow rate measurement data [31]. Within uncertainty limits, some authors predicted that the variation of the flow between inlet and outlet will generally decrease. This statement is an acceptable prediction and it will discover the weakness of MRI flow measurement in the boundary condition setup. In the present investigation, the significance of the right flow rate is stressed. During a systole and diastole cycle, the CBA diameter can suddenly change more than 17% of the results, especially in the diastolic condition [55]. This is because there has no agreement in the error of flow rate, especially in the MRI velocity measurement results. Besides, the agreement from Zhao et al. [12] for the CFD flow simulation can be realized successfully in the CBA studies. The results showed that the velocity profile changes corresponded to the findings of the former researchers. The main concern of the mentioned techniques is to reduce the computational cost of the integration between PC-MRI and CFD.

Boundary Condition for CFD Setup

In the CFD simulation, the critical step is to set the boundary condition for inflow and outflow. The boundary condition setup for CFD simulation is crucial for obtaining simulation results such as velocity flow field and WSS distribution with low deviation as compared to the MRI measurement [25]. Through the blood flow in the CFD simulation, there are three types of physical boundary setup and the wall setup is the common type. By setting zero in the velocity components (*no-slip condition*), there is no flow velocity acceptable via the wall of the blood vessel. The previous review is briefly described in Table 4**.**

Inlet Boundary Condition

Generally, the inlet boundary condition is given at the upstream side of CBAs, with an unrealistic profile such as a flat/straight, completely established or based on time-varying velocity data gathered from PC-MRI. Mainly, the flat/straight velocity distribution is used together in the transient studies. The hypothesis regarding to the straight velocity profile lines at CBA inlets has been clarified through numerous in vivo conditions [56–59]. Furthermore, with the omission of Morbiducci et al. [60] and Renner et al. [61], there is no study investigating the consequence of different inlet velocity profiles and describing its outcome in the other CBAs [62–65]. Morbiducci et al. [60] examined the impact of straight and complete developed inlet velocity profiles on the patient-specific CFD hemodynamics and compared them to the PC-MRI integrated CFD velocity flow data. The achieved outcomes were compared to the distribution of WSS. It was reported that the obligation of PC-MRI data on velocity profiles at the inlet may require to concern shear stress behaviour for satisfactory precision. There are three main boundary conditions involving CFD with PC-MRI velocity measurements: a uniform inflow, a developed inflow, and an inflow set corresponding to the MRI velocity measurements [31]. There is no physiological but long inflow is required for the first boundary condition study, the second boundary

condition decreases central processing unit (CPU) time expressively but more understanding is needed on how to develop the flow, and the third boundary condition can also decrease the CPU time region sequence if the procurement position is close to the interest area of study. In the general flow area, the option of filtering for different geometry (thresholds) has been shown to create similar results.

Outlet Boundary Condition

In physical conditions, the branches of CBAs are linking with smaller vessels. It is impossible to locate most of the bifurcation in the simulation and the model has to be completed at some stage depending on the study's specific objective. Additionally, such divisions must be interpreted into the correct terminal description and thus, the characteristics of CBAs can be practically characterized. Formerly, the outlet boundary conditions for CFD analysis of CBAs were approved with constant or time-varying pressures, normally as zero. Moreover, the simulations could not be achieved where the flow and pressure fields are parts of the preferred solutions [66, 67]. However, Gallo et al. [68] lately investigated the effects on the obligation of personalized PC-MRI measurement by defining blood flow rates as outlet boundary conditions. In order to gain physiologically accurate outcomes, the restrained flow rates have to be executed at 75% of the carotid artery model outlets. Nevertheless, there is no practical estimation of this flow ratio for patient-specific Fluid-Structure Interaction (FSI) models and also motivation adhering to the constant flow through the arch branches during the whole cardiac cycle [69].

VALIDATION ON INTEGRATED PC-MRI AND CFD

PC-MRI is a 3D imaging that allows a non-invasive and accurate assessment of vessel as well as the blood flow field in all vessels. The inflow and outflow of a vessel segment can be assessed through the velocity from PC-MRI [70]. When the boundary conditions are obtainable, a comparison of blood flow can be studied by using PC-MRI integrated CFD as illustrated in Figure 2. Through the velocity from PC-MRI, the flow during numerous phases in the cardiac cycle can be assessed with a medium systematic error. These have been mainly used at in vitro geometrical models [71], [72] when comparing to the CFD validation studies. From Kung et al. [73], their study has related to numerical analysis of blood flow and pressure distribution including vessel wall deformation under physiological flow condition. Concerning the in vivo validation, some comparative studies have been comparing patient-specific CFD with PC-MRI measurements [71, 74, 75]. For patient-specific intracranial aneurysms problems, Boussel et al. [76] have conducted a comparison between CFD and PC-MRI measurement.
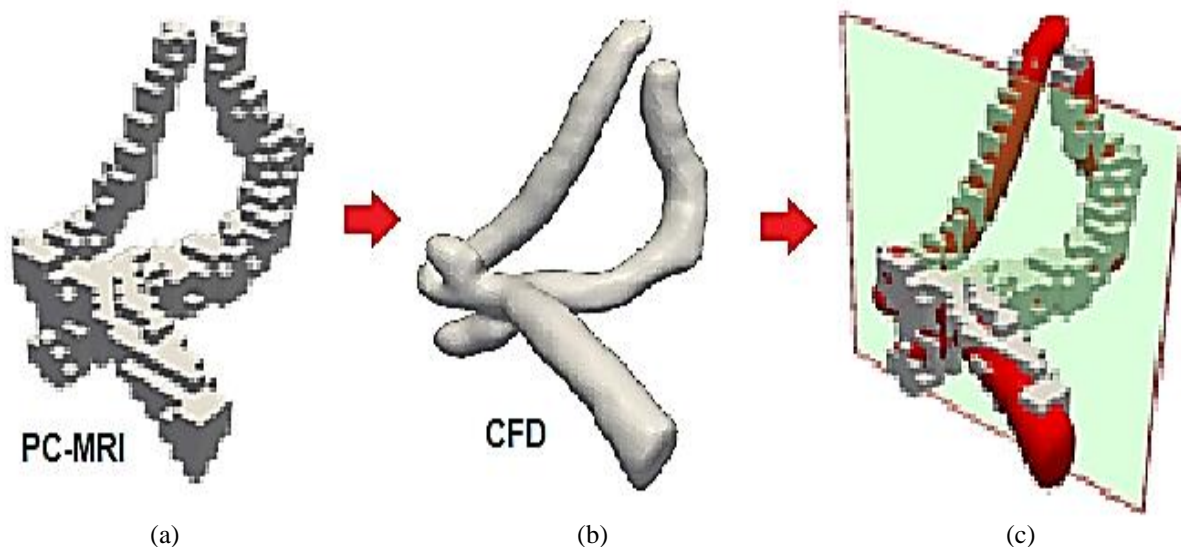

| (a) | (b) | (c) |

Figure 3. (a) PC-MRI image; (b) DSA image (Used for CFD Simulation); (c) Integrated MRI mesurement and CFD simulation for analysis

Table 3. Overview of measurement parameter and PC-MRI setup from the previous studies

Author	Focus Area						Software	PC-MRI				
	CBA	IA	WSS	V V	V P	Streamline		Data Size	Slice Thickness	Velocity Encoding	TR/TE	FOV
Jonas et al. [77]	O	×	×	O	O	O	1.5T Philips Achieva	O	O	O	40/- ms	10cm
Masao et al. [78]	×	O	O	×	O	O	O	256x256x60	1.5mm	40cm/s	O	O
Quan et al. [13]	×	O	×	O	×	O	1.5T Signa	256x256x21	1.5mm	100cm/s	45/8.7ms	12cm
Ooij et al. [79]	O	×	O	×	×	O	3T Philips Healthcare	200x200x92	O	70cm/s	21/4.2ms	22cm
Jing et al. [80]	×	O	×	×	O	O	1.5T Signa	525x525x25	O	500cm/s	14/3.6ms	16cm
Haruo et al. [81]	O	×	×	×	O	×	1.5T Signa	160x160x32	O	100cm/s	40/2.2ms	32 cm
Loic et al. [82]	O	×	×	O	×	O	1.5T Philips Achieva	512x512x90	1.2mm	O	50/2.0ms	24cm
Sebastian et al. [83]	×	O	O	×	O	×	3.0T Siemens	O	O	15cm/s	O	O
Long et al. [18]	×	O	×	×	×	O	1.5T Signa	256x256x128	1.5mm	50cm/s	45/7.5ms	28cm
Kohler et al. [84]	×	O	×	O	O	O	1.5T Signa	256x256x100	0.9mm	100cm/s	25/6.0ms	18cm
Glor et al. [31]	×	O	O	O	×	O	1.5T Philips Medical	256x256x120	5.0mm	O	19/9.4ms	16cm
Ooij et al.[85]	O	×	O	O	×	O	1.5T Philips Medical	200x200x30	O	100cm/s	11/3.9ms	25cm
Zhao et al. [86]	×	O	O	O	×	O	1.5T Signa	256x256x128	1.05mm	110cm/s	25/7.0ms	13cm
Papathanasopoulou et al. [87]	×	O	×	O	O	O	1.5T Signa	256x256x128	1.05mm	110cm/s	25/6.5ms	13cm
Marshall et al. [88]	×	O	×	×	O	O	1.5T Signa	O	1.40mm	120cm/s	O	O

×: available, ○: not available, **CBA:** carotid bifurcation artery, **IA:** intracranial aneurysm, **WSS:** wall shear stress, **VV:** velocity vector, **VP:** velocity profile, **TR:** repetition time, **TE:** echo time, **FOV:** field of view.

Table 4. Overview of CFD setup from the previous studies

Author	Focus Area		CFD										Equation (Fluid Flow)		
	CBA	IA	Software	Viscosity (kg/ms)	Density (kg/m³)	Total Element	Mesh Type		Rigid Wall	Steady State	Newtonian	Incom-pressible	NSE	CE	GE
							Tetrahedral	Hexahedral							
Jonas et al. [77]	O	×	CFX 14.5	0.0040	1050	O	O	O	O	O	O	O	×	O	×
Masao et al. [78]	×	O	Fluent 5.0	0.0045	1055	O	O	O	×	×	O	×	×	×	O
Quan et al. [13]	×	O	CFX 4.2	0.0040	1050	O	O	O	×	O	×	×	O	O	O
Ooij et al. [79]	O	×	Fluent 6.3	0.0040	1063	2608270	×	O	O	×	O	×	O	×	O
Jing et al. [80]	×	O	Fluent 12.0	0.0035	1050	O	×	O	O	O	×	×	×	×	O
Haruo et al. [81]	O	×	ACUSIM	0.0038	1054	753178	×	O	O	O	×	×	O	O	O
Loic et al. [82]	O	×	Fluent 12.0	0.0035	1054	O	×	O	×	O	×	O	O	O	O
Sebastian et al. [83]	×	O	COSMOL Multiphysics	0.0040	1060	O	O	O	O	O	×	×	O	O	O
Long et al. [18]	×	O	CFX 4.0	0.0040	1054	O	O	O	O	O	×	O	×	O	O
Kohler et al. [84]	×	O	CFX 4.0	0.0033	1050	O	O	O	×	×	O	×	×	×	×
Glor et al. [31]	×	O	PAMFLOW-GEN 3D (ESI Software)	0.0010	998	O	×	O	O	×	×	×	×		×
Ooij et al. [85]	O	×	Fluent 12.0	0.0010	1000	O	O	O	×	×	O	O	×	O	O
Zhao et al. [86]	×	O	CFX 4.0	0.0038	1020	41600	O	×	O	×	O	O	×	O	×
Papathanasopoulou et al. [87]	×	O	CFX 4.0	0.0038	1020	41600	O	×	×	×	O	O	×	O	×
Marshall et al. [88]	×	O	CFX 4.0	0.0035	1050	42000	O	×	×	O	O	O	×	O	O

× : available, ○: not available, **CBA:** carotid bifurcation artery, **IA:** intracranial aneurysm, **WSS:** wall shear stress, **VV:** velocity vector, **VP:** velocity profile, **CFD:** computational fluid dynamics, **NSE:** Navier Stokes equation, **CE:** continuity equation, **GE:** governing equation

Most of the velocity findings were slightly different to PC-MRI data calculated at various parts of the CBAs which were not used as the boundary conditions [89–94]. The reported CFD simulation findings did not agree well with PC-MRI integrated CFD in velocity forms. In ther words, the prediction still does not show that the velocity flow is correctly assumed but it gives some good potential to the first step towards validation and verification. Besides, the validation studies may likely involve the achievement of more measurement data but additional computational cost is the critical value on CFD simulation based on the results in the future study. From Zhao et al. [86], the authors reported that good qualitative agreement was shown in CBAs phantom under a pulsatile flow condition with some quantitative difference between PC-MRI and CFD but still, there was low agreement on WSS distribution at intracranial aneurysms between PC-MRI and CFD. Moreover, the configuration and position of shearing velocity in PC-MRI integrated with CFD were similar in term of flow direction as reported by Isoda et al. [95]. Furthermore, Mohd Adib et al., [96] claimed that low-velocity difference was achieved with velocity-field-optimized (V-optimized) approach and they also introduced a physically consistent feedback control-based data assimilation (PFC-DA) method [97] to improve blood flow analysis by coupling the body force with the pressure boundary condition, but there was still 20% of deviation on the velocity difference.

FUTURE RECOMMENDATION

The blood flow study enhancement through integrated between MRI measurement and CFD simulation with several aspects in terms of model geometry, mesh generation, and boundary condition were investigated in this article. All of the computational, numerical and simulation approaches were considered in this paper. The existing approach emerges primarily from a physical point of view, thus the mathematical reliability is still not adequately vindicated. It is confirmed that the variations in treating boundaries affect the velocity flow field abd WSS distributions in CBAs. In this paper, we have explained the current approach based on some numerical studies. In future, this research can be extended to examine the current formulation in a pearl of mathematical wisdom towards a unique direction of the data assimilation based blood flow analysis.

CONCLUSION

CFD has expanded great significance in understanding and investigating human diseases. However, as noted previously, the level of difficulty to get the result requires more information such as characteristics of the mechanical behavior (mass flow rate) from PC-MRI and setup of boundary conditions from the CFD. Unfortunately, some bits of intelligence presented the result by trial and error. Many physicians do not have all the specific equipment required to assess the multiple tasks in a short time and also to plan the optimal corrective techniques estimating the patient's result for a given diagnosis which is only based on CT-scan and MRI images [34]. So, this perspective review aims to extend computational work contributing to continuous development of human health with robust cooperation and collaboration between clinicians and engineers.

ACKNOWLEDGEMENT

REFERENCES

[1]   H. Luo, J. D. Baum, and R. Lo, "An accurate , fast , matrix-free implicit method for computing unsteady flows on unstructured grids," vol. 30, pp. 137–159, 2001.

[2]   X. Lin, X. Li, and X. Lin, "A Review on Applications of Computational Methods," no. July, pp. 1–17, 2020.

[3]   I. Balashazy, T. Heistracher, and W. Hofmann, "Air Flow and Particle Deposition Patterns in Bronchial Airway Bifurcations: The Effect of Different CFD Models and Bifurcation Geometries," *J. Aerosol Med.*, vol. 9, no. 3, pp. 287–301, Jan. 1996, doi: 10.1089/jam.1996.9.287.

[4]   P. Verdonck and K. Perktold, *Intra and Extracorporeal Cardiovascular Fluid Dynamics - 2 Volume Set*, Advances i. Southampton SO40 7AA, United Kingdom.: WIT Press, 2000.

[5]   S. J. Sherwin *et al.*, "The Influence of Out-of-Plane Geometry on the Flow Within a Distal End-to-Side Anastomosis ," *J. Biomech. Eng.*, vol. 122, no. 1, pp. 86–95, Jul. 1999, doi: 10.1115/1.429630.

[6]   T. Ebbers, L. Wigstro, A. F. Bolger, J. Engvall, and M. Karlsson, "Estimation of Relative Cardiovascular Pressures Using Time-Resolved Three-Dimensional Phase Contrast MRI," vol. 879, pp. 872–879, 2001.

[7]   S. Prakash and C. R. Ethier, "Requirements for Mesh Resolution in 3D Computational Hemodynamics ," *J. Biomech. Eng.*, vol. 123, no. 2, pp. 134–144, Dec. 2000, doi: 10.1115/1.1351807.

[8]   B. Condon and D. M. Hadley, "Potential MR Hazard to Patients With Metallic Heart Valves : The Lenz Effect," vol. 176, pp. 171–176, 2000.

[9]   N. B. Wood *et al.*, "Combined MR Imaging and CFD Simulation of Flow in the Human Descending Aorta," vol. 713, pp. 699–713, 2001.

[10]   J. Wang *et al.*, "Carotid Bifurcation With Tandem Stenosis—A Patient-Specific Case Study Combined in vivo Imaging, in vitro Histology and in silico Simulation," *Front. Bioeng. Biotechnol.*, vol. 7, no. November, pp. 1–11, 2019, doi: 10.3389/fbioe.2019.00349.

[11]   N. H. Johari *et al.*, "Disturbed Flow in a Stenosed Carotid Artery Bifurcation: Comparison of RANS-Based Transitional Model and les with Experimental Measurements," *Int. J. Appl. Mech.*, vol. 11, no. 4, pp. 1–21, 2019, doi: 10.1142/S1758825119500327.

[12]   S. Z. Zhao *et al.*, "Blood flow and vessel mechanics in a physiologically realistic model of a human carotid arterial bifurcation," *J. Biomech.*, vol. 33, no. 8, pp. 975–984, 2000, doi: 10.1016/S0021-9290(00)00043-9.

[13]   Q. Long, X. Y. Xu, B. Ariff, S. A. Thom, A. D. Hughes, and A. V Stanton, "Reconstruction of Blood Flow Patterns in a Human Carotid Bifurcation : A Combined CFD and MRI Study," vol. 311, pp. 299–311, 2000.

[14]   H. M. Ladak, J. S. Milner and, and D. A. Steinman, "Rapid Three-Dimensional Segmentation of the Carotid Bifurcation From Serial MR Images," *J. Biomech. Eng.*, vol. 122, no. 1, pp. 96–99, Aug. 1999, doi: 10.1115/1.429646.

[15]   J. S. Milner, J. A. Moore, B. K. Rutt, and D. A. Steinman, "Hemodynamics of human carotid artery bifurcations : Computational studies with models reconstructed from magnetic resonance imaging of normal subjects," pp. 143–156, 1998.

[16]   J. Thomas, J. Milner, and D. Steinman, "On the Influence of Vessel Planarity on Local Hemodynamics At the Human Carotid Bifurcation," *Biorheology*, vol. 39, pp. 443–448, Feb. 2002.

[17]   J. R. Cebral, P. J. Yim, R. Loehner, O. Soto, H. Marcos, and P. L. Choyke, "New methods for computational fluid dynamics modeling of carotid artery from magnetic resonance angiography," in *Proc.SPIE*, May 2001, vol. 4321, [Online]. Available: https://doi.org/10.1117/12.428135.

[18]   Q. Long, X. Y. Xu, M. Bourne, and T. M. Griffith, "Numerical Study of Blood Flow in an Anatomically Realistic Aorto-Iliac Bifurcation Generated From MRI Data," vol. 576, pp. 565–576, 2000.

[19]   Q. Long, X. Y. Xu, M. W. Collins, M. Bourne, and T. M. Griffith, "Magnetic resonance image processing and structured grid generation of a human abdominal bifurcation," *Comput. Methods Programs Biomed.*, vol. 56, no. 3, pp. 249–259, 1998, doi: https://doi.org/10.1016/S0169-2607(98)00008-X.

[20]   Q. Long, X. Y. Xu, M. W. Collins, T. M. Griffith, and M. Bourne, "The combination of magnetic resonance angiography and computational fluid dynamics: a critical review.," *Crit. Rev. Biomed. Eng.*, vol. 26, no. 4, pp. 227–274, 1998, doi: 10.1615/critrevbiomedeng.v26.i4.10.

[21]   X. Y. Xu, Q. Long, M. W. Collins, M. Bourne, and T. M. Griffith, "Reconstruction of blood flow patterns in human arteries," *Proc. Inst. Mech. Eng. Part H J. Eng. Med.*, vol. 213, no. 5, pp. 411–421, May 1999, doi: 10.1243/0954411991535022.

[22]   A. Spilt *et al.*, "Reproducibility of total cerebral blood flow measurements using phase contrast magnetic resonance imaging," *J. Magn. Reson. Imaging*, vol. 16, no. 1, pp. 1–5, 2002, doi: 10.1002/jmri.10133.

[23]   S. Prevrhal, C. H. Forsythe, R. J. Harnish, M. Saeed, and B. M. Yeh, "CT angiographic measurement of vascular blood flow velocity by using projection data," *Radiology*, vol. 261, no. 3, pp. 923–929, 2011, doi: 10.1148/radiol.11110617.

[24]   L. Sheh Hong, M. Azrul Hisham Mohd Adib, M. Uzair Matalif, M. Shafie Abdullah, N. Hartini Mohd Taib, and R. Hassan, "Modeling and Simulation of Blood Flow Analysis on Simplified Aneurysm Models," *IOP Conf. Ser. Mater. Sci. Eng.*, vol. 917, p. 012067, 2020, doi: 10.1088/1757-899x/917/1/012067.

[25]   S. H. Lim, M. A. H. Mohd Adib, M. Abdullah, and R. Hassan, "Qualitative and Quantitative Comparison of Hemodynamics Between MRI Measurement and CFD Simulation on Patient-specific Cerebral Aneurysm – A Review," *J. Adv. Res. Fluid Mech. Therm. Sci.*, vol. 68, pp. 112–123, Mar. 2020, doi: 10.37934/arfmts.68.2.112123.

[26]   K. H. Parker and C. G. Caro, "Flow in the macrocirculation: basic concepts from fluid mechanics," *Magn. Reson. Angiogr. concepts Appl. St. Louis Mosby*, pp. 134–145, 1992.

[27]   C. A. Taylor and D. A. Steinman, "Image-based modeling of blood flow and vessel wall dynamics: Applications, methods and future directions: Sixth international bio-fluid mechanics symposium and workshop, March 28-30, 2008 Pasadena, California," *Ann. Biomed. Eng.*, vol. 38, no. 3, pp. 1188–1203, 2010, doi: 10.1007/s10439-010-9901-0.

[28]   R. J. Van Der Geest, A. De Roos, E. E. Van Der Wall, and J. H. C. Reiber, "Quantitative analysis of cardiovascular MR images," *Int. J. Card. Imaging*, vol. 13, no. 3, pp. 247–258, 1997, doi: 10.1023/A:1005869509149.

[29]   J. R. Cebral and R. Löhner, "From medical images to anatomically accurate finite element grids," *Int. J. Numer. Methods Eng.*, vol. 51, no. 8, pp. 985–1008, Jul. 2001, doi: 10.1002/nme.205.

[30]   J. A. Moore, D. A. Steinman, and C. R. Ethier, "Computational blood flow modelling: Errors associated with reconstructing finite element models from magnetic resonance images," *J. Biomech.*, vol. 31, no. 2, pp. 179–184, 1997, doi: 10.1016/S0021-9290(97)00125-5.

[31]   F. P. Glor, J. J. M. Westenberg, J. Vierendeels, M. Danilouchkine, and P. Verdonck, "Validation of the Coupling of Magnetic Resonance Imaging Velocity Measurements with Computational Fluid Dynamics in a U Bend," *Artif. Organs*, vol. 26, no. 7, pp. 622–635, Jul. 2002, doi: 10.1046/j.1525-1594.2002.07085.x.

[32]   S. J. Weston, N. B. Wood, G. Tabor, A. D. Gosman, and D. N. Firmin, "Combined MRI and CFD analysis of fully developed steady and pulsatile laminar flow through a bend," *J. Magn. Reson. Imaging*, vol. 8, no. 5, pp. 1158–1171, Sep. 1998, doi: 10.1002/jmri.1880080523.

[33]   R. Botnar, G. Rappitsch, M. Beat Scheidegger, D. Liepsch, K. Perktold, and P. Boesiger, "Hemodynamics in the carotid artery bifurcation: A comparison between numerical simulations and in vitro MRI measurements," *J. Biomech.*, vol. 33, no. 2, pp. 137–144, 2000, doi: 10.1016/S0021-9290(99)00164-5.

[34]   A. D. Caballero and S. Laín, "A Review on Computational Fluid Dynamics Modelling in Human Thoracic Aorta," *Cardiovasc. Eng. Technol.*, vol. 4, no. 2, pp. 103–130, 2013, doi: 10.1007/s13239-013-0146-6.

[35]   C. G. Caro, T. J. Pedley, R. C. Schroter, and W. A. Seed, *The Mechanics of the Circulation*. Oxford University Press, 1978.

[36]   F. M. A. Box, R. J. Van Der Geest, M. C. M. Rutten, and J. H. C. Reiber, "The influence of flow, vessel diameter, and non-Newtonian blood viscosity on the wall shear stress in a carotid bifurcation model for unsteady flow," *Invest. Radiol.*, vol. 40, no. 5, pp. 277–294, 2005, doi: 10.1097/01.rli.0000160550.95547.22.

[37]   C. C. Hamakiotes and S. A. Berger, "Periodic flows through curved tubes: the effect of the frequency parameter," *J. Fluid Mech.*, vol. 210, pp. 353–370, 1990, doi: DOI: 10.1017/S002211209000132X.

[38]   Y. Komai and K. Tanishita, "Fully developed intermittent flow in a curved tube," *J. Fluid Mech.*, vol. 347, pp. 263–287, 1997, doi: DOI: 10.1017/S0022112097006538.

[39]   T. Naruse and K. Tanishita, "Large Curvature Effect on Pulsatile Entrance Flow in a Curved Tube: Model Experiment Simulating Blood Flow in an Aortic Arch," *J. Biomech. Eng.*, vol. 118, no. 2, pp. 180–186, May 1996, doi: 10.1115/1.2795957.

[40]   a Santamarina, E. Weydahl, J. M. Siegel, and J. E. Moore, "Computational Analysis of Flow in a Curved Tube Model of the Coronary Arteries Effects of Time-varying Curvature," *Ann. Biomed. Eng.*, vol. 26, pp. 944–954, 1998.

[41]   D. A. Steinman, "Image-based computational fluid dynamics modeling in realistic arterial geometries," *Ann. Biomed. Eng.*, vol. 30, no. 4, pp. 483–497, 2002, doi: 10.1114/1.1467679.

[42]   M. Sumida, K. Sudou, and H. Wada, "Pulsating Flow in a Curved Pipe (Secondary Flow)," *JSME Int. journal. Ser. 2, Fluids Eng. heat Transf. power, Combust. Thermophys. Prop.*, vol. 32, pp. 523–531, Nov. 1989, doi: 10.1299/jsmeb1988.32.4_523.

[43]   S. L. Waters and T. J. Pedley, "Oscillatory flow in a tube of time-dependent curvature. Part 1. Perturbation to flow in a stationary curved tube," *J. Fluid Mech.*, vol. 383, pp. 327–352, 1999, doi: DOI: 10.1017/S0022112099004085.

[44]   P. W. Longest and S. Vinchurkar, "Effects of mesh style and grid convergence on particle deposition in bifurcating airway models with comparisons to experimental data," *Med. Eng. Phys.*, vol. 29, no. 3, pp. 350–366, 2007, doi: 10.1016/j.medengphy.2006.05.012.

[45]   O. Sahni, K. E. Jansen, M. S. Shephard, C. A. Taylor, and M. W. Beall, "Adaptive boundary layer meshing for viscous flow simulations," *Eng. Comput.*, vol. 24, no. 3, pp. 267–285, 2008, doi: 10.1007/s00366-008-0095-0.

[46]   J. Chen and X.-Y. Lu, "Numerical investigation of the non-Newtonian pulsatile blood flow in a bifurcation model with a non-planar branch," *J. Biomech.*, vol. 39, no. 5, pp. 818–832, 2006, doi: https://doi.org/10.1016/j.jbiomech.2005.02.003.

[47]   B. M. Johnston, P. R. Johnston, S. Corney, and D. Kilpatrick, "Non-Newtonian blood flow in human right coronary arteries: steady state simulations," *J. Biomech.*, vol. 37, no. 5, pp. 709–720, 2004, doi: https://doi.org/10.1016/j.jbiomech.2003.09.016.

[48]   D. Liepsch, "An introduction to biofluid mechanics—basic models and applications," *J. Biomech.*, vol. 35, no. 4, pp. 415–435, 2002, doi: https://doi.org/10.1016/S0021-9290(01)00185-3.

[49]   B. M. Johnston, P. R. Johnston, S. Corney, and D. Kilpatrick, "Non-Newtonian blood flow in human right coronary arteries: Transient simulations," *J. Biomech.*, vol. 39, no. 6, pp. 1116–1128, 2006, doi: https://doi.org/10.1016/j.jbiomech.2005.01.034.

[50]   B. S. Narang, "Exact solution for entrance region flow between parallel plates," *Int. J. Heat Fluid Flow*, vol. 4, no. 3, pp. 177–181, 1983, doi: 10.1016/0142-727X(83)90066-8.

[51]   C. Y. Wang, "Exact Solutions of the Steady-State Navier-Stokes Equations," *Annu. Rev. Fluid Mech.*, vol. 23, no. 1, pp. 159–177, 1991, doi: 10.1146/annurev.fl.23.010191.001111.

[52]   X. Liu, F. Pu, Y. Fan, X. Deng, D. Li, and S. Li, "A numerical study on the flow of blood and the transport of LDL in the human aorta: The physiological significance of the helical flow in the aortic arch," *Am. J. Physiol. - Hear. Circ. Physiol.*, vol. 297, no. 1, pp. 163–170, 2009, doi: 10.1152/ajpheart.00266.2009.

[53]   T. J. Pedley, *The Fluid Mechanics of Large Blood Vessels*. Cambridge: Cambridge University Press, 1980.

[54]   S. Lownie, W. Kalata, F. Loth, and D. W. Holdsworth, *PIV-Measured Versus CFD-Predicted Flow Dynamics in Anatomically Realistic Cerebral Aneurysm Models*, no. May. 2008.

[55]   R. S. Reneman, A. P. G. Hoeks, and N. Westerhof, "Non-invasive assessment of artery wall properties in humans-methods and interpretation," *J Vasc Invest*, vol. 2, no. 2, pp. 53–64, 1996.

[56]   B. H. L. Falserri, K. M. Kiser, G. P. Francis, and E. R. Belmore, "Sequential Velocity Development in the Ascending and Descending Aorta of the Dog," vol. XXXI, pp. 328–338, 1972.

[57]   X. He and D. N. Ku, "Pulsatile Flow in the Human Left Coronary Artery Bifurcation: Average Conditions," *J. Biomech. Eng.*, vol. 118, no. 1, pp. 74–82, Feb. 1996, doi: 10.1115/1.2795948.

[58] R. M. Nerem, J. A. Rumberger JR, D. R. Gross, W. W. Muir, and G. L. Geiger, "Hot film coronary artery velocity measurements in horses1," *Cardiovasc. Res.*, vol. 10, no. 3, pp. 301–313, May 1976, doi: 10.1093/cvr/10.3.301.

[59] W. A. Seed and N. B. Wood, "Velocity patterns in the aorta1," *Cardiovasc. Res.*, vol. 5, no. 3, pp. 319–330, Jul. 1971, doi: 10.1093/cvr/5.3.319.

[60] U. Morbiducci, R. Ponzini, D. Gallo, C. Bignardi, and G. Rizzo, "Inflow boundary conditions for image-based computational hemodynamics : Impact of idealized versus measured velocity profiles in the human aorta," *J. Biomech.*, vol. 46, no. 1, pp. 102–109, 2013, doi: 10.1016/j.jbiomech.2012.10.012.

[61] J. Renner, D. Loyd, T. Länne, and M. Karlsson, "Is a Flat Inlet Profile Sufficient for WSS Estimation in the Aortic Arch ? Is a Flat Inlet Profile Sufficient for WSS Estimation in the Aortic Arch ?," no. May 2014, 2008.

[62] I. C. Campbell, J. Ries, S. S. Dhawan, A. A. Quyyumi, W. R. Taylor, and J. N. Oshinski, "Effect of Inlet Velocity Profiles on Patient-Specific Computational Fluid Dynamics Simulations of the Carotid Bifurcation," *J. Biomech. Eng.*, vol. 134, no. 5, May 2012, doi: 10.1115/1.4006681.

[63] L. Morris, P. Delassus, P. Grace, F. Wallis, M. Walsh, and T. Mcgloughlin, "Effects of flat, parabolic and realistic steady flow inlet profiles on idealised and realistic stent graft fits through Abdominal Aortic Aneurysms (AAA)," *Med. Eng. Phys.*, vol. 28, pp. 19–26, Feb. 2006, doi: 10.1016/j.medengphy.2005.04.012.

[64] K. Moyle, L. Antiga, and D. Steinman, "Inlet Conditions for Image-Based CFD Models of the Carotid Bifurcation: Is it Reasonable to Assume Fully Developed Flow?," *J. Biomech. Eng.*, vol. 128, pp. 371–379, Jul. 2006, doi: 10.1115/1.2187035.

[65] J. G. M. Yers, J. A. M. Oore, M. O. Jha, K. W. J. Ohnston, and C. R. E. Thier, "Factors Influencing Blood Flow Patterns in the Human Right Coronary Artery," vol. 29, pp. 109–120, 2001, doi: 10.1114/1.1349703.

[66] J.-F. Gerbeau, M. Vidrascu, and P. Frey, "Fluid–structure interaction in blood flows on geometries based on medical imaging," *Comput. Struct.*, vol. 83, no. 2, pp. 155–165, 2005, doi: https://doi.org/10.1016/j.compstruc.2004.03.083.

[67] F. N. V. A. N. D. E. Vosse, J. D. E. Hart, D. Bessems, and A. Segal, "Finite-element-based computational methods for cardiovascular fluid-structure interaction," pp. 335–368, 2003.

[68] D. Gallo *et al.*, "On the Use of In Vivo Measured Flow Rates as Boundary Conditions for Image-Based Hemodynamic Models of the Human Aorta: Implications for Indicators of Abnormal Flow," *Ann. Biomed. Eng.*, vol. 40, no. 3, pp. 729–741, 2012, doi: 10.1007/s10439-011-0431-1.

[69] C. H. A. T. Aylor, C. H. P. C. Heng, L. E. A. E. Spinosa, B. E. T. T. Ang, D. A. P. Arker, and R. O. J. H. Erfkens, "In Vivo Quantification of Blood Flow and Wall Shear Stress in the Human Abdominal Aorta During Lower Limb Exercise," vol. 30, pp. 402–408, 2002, doi: 10.1114/1.1476016.

[70] E. J. Bekkers and C. A. Taylor, "Multiscale Vascular Surface Model Generation From Medical Imaging Data Using Hierarchical Features," *IEEE Trans. Med. Imaging*, vol. 27, no. 3, pp. 331–341, 2008.

[71] M. D. Ford *et al.*, "Virtual angiography for visualization and validation of computational models of aneurysm hemodynamics," *IEEE Trans. Med. Imaging*, vol. 24, no. 12, pp. 1586–1592, 2005, doi: 10.1109/TMI.2005.859204.

[72] J. P. K. U. Oy, C. H. J. E. Lkins, and C. H. A. T. Aylor, "Comparison of CFD and MRI Flow and Velocities in an In Vitro Large Artery Bypass Graft Model," vol. 33, no. 3, pp. 257–269, 2005, doi: 10.1007/s10439-005-1729-7.

[73] R. Y. A. N. B. W. Icker, M. I. V. M. C. C. Onnell, and C. H. A. T. Aylor, "In Vitro Validation of Finite Element Analysis of Blood Flow in Deformable Models," vol. 39, no. 7, pp. 1947–1960, 2011, doi: 10.1007/s10439-011-0284-7.

[74] N. O. J. P. Elc, C. H. K. Z. Arins, and C. H. A. T. Aylor, "In Vivo Validation of Numerical Prediction of Blood Flow in Arterial Bypass Grafts," vol. 30, pp. 743–752, 2002, doi: 10.1114/1.1496086.

[75] V. L. Rayz *et al.*, "Numerical Simulations of Flow in Cerebral Aneurysms: Comparison of CFD Results and In Vivo MRI Measurements," *J. Biomech. Eng.*, vol. 130, no. 5, Aug. 2008, doi: 10.1115/1.2970056.

[76] L. Boussel *et al.*, "Phase-Contrast Magnetic Resonance Imaging Measurements in Intracranial Aneurysms In Vivo of Flow Patterns , Velocity Fields , and Wall Shear Stress : Comparison with Computational Fluid Dynamics," vol. 417, pp. 409–417, 2009, doi: 10.1002/mrm.21861.

[77] J. Lantz and T. Ebbers, "A new method for obtaining high-resolution velocity data from magnetic resonance imaging?," 2013, no. Cmiv, p. 2012, [Online]. Available: http://www.malmokongressbyra.se/kongress/download/mtd/1d1.pdf.

[78] M. Watanabe, R. Kikinis, and C.-F. Westin, "Level set-based integration of segmentation and computational fluid dynamics for flow correction in phase contrast angiography," *Acad. Radiol.*, vol. 10, no. 12, pp. 1416–1423, Dec. 2003, doi: 10.1016/S1076-6332(03)00509-9.

[79] P. van Ooij *et al.*, "Complex flow patterns in a real-size intracranial aneurysm phantom: phase contrast MRI compared with particle image velocimetry and computational fluid dynamics," *NMR Biomed.*, vol. 25, no. 1, pp. 14–26, Jan. 2012, doi: 10.1002/nbm.1706.

[80] J. Jiang, K. Johnson, K. Valen-Sendstad, K.-A. Mardal, O. Wieben, and C. Strother, "Flow characteristics in a canine aneurysm model: A comparison of 4D accelerated phase-contrast MR measurements and computational fluid dynamics simulations," *Med. Phys.*, vol. 38, no. 11, pp. 6300–6312, Nov. 2011, doi: 10.1118/1.3652917.

[81] H. Isoda *et al.*, "Comparison of hemodynamics of intracranial aneurysms between MR fluid dynamics using 3D cine phase-contrast MRI and MR-based computational fluid dynamics," pp. 913–920, 2010, doi: 10.1007/s00234-009-0634-4.

[82] L. Boussel *et al.*, "Phase-contrast magnetic resonance imaging measurements in intracranial aneurysms in vivo of flow patterns, velocity fields, and wall shear stress: Comparison with computational fluid dynamics," *Magn. Reson. Med.*, vol. 61, no. 2, pp. 409–417, 2009, doi: 10.1002/mrm.21861.

[83]   S. Meier, A. Nennemuth, N. Tchipev, A. Harloff, M. Markl, and T. Preusser, "Towards Patient-Individual Blood Flow Simulations based on PC-MRI Measurements," 2011.

[84]   U. PhD, I. Marshall, M. PhD, Q. Long, X. Xu, and P. Hoskins, "MRI Measurement of wall shear stress vectors in bifurcation models and comparison with CFD predictions," *J. Magn. Reson. Imaging*, vol. 14, pp. 563–573, Oct. 2001, doi: 10.1002/jmri.1220.

[85]   P. Van Ooij, J. J. Schneiders, H. A. Marquering, C. B. Majoie, E. Van Bavel, and A. J. Nederveen, "3D cine phase-contrast MRI at 3T in intracranial aneurysms compared with patient-specific computational fluid dynamics," *Am. J. Neuroradiol.*, vol. 34, no. 9, pp. 1785–1791, 2013, doi: 10.3174/ajnr.A3484.

[86]   S. Z. Z. Hao, P. P. Apathanasopoulou, Q. L. Ong, and I. M. Arshall, "Comparative Study of Magnetic Resonance Imaging and Image-Based Computational Fluid Dynamics for Quantification of Pulsatile Flow in a Carotid Bifurcation Phantom," vol. 31, pp. 962–971, 2003, doi: 10.1114/1.1590664.

[87]   P. Papathanasopoulou *et al.*, "MRI measurement of time-resolved wall shear stress vectors in a carotid bifurcation model, and comparison with CFD predictions," *J. Magn. Reson. Imaging*, vol. 17, no. 2, pp. 153–162, 2003, doi: 10.1002/jmri.10243.

[88]   I. Marshall, S. Zhao, P. Papathanasopoulou, P. Hoskins, and X. Y. Xu, "MRI and CFD studies of pulsatile flow in healthy and stenosed carotid bifurcation models," *J. Biomech.*, vol. 37, no. 5, pp. 679–687, 2004, doi: 10.1016/j.jbiomech.2003.09.032.

[89]   S. Jin, J. Oshinski, and D. P. Giddens, "Effects of Wall Motion and Compliance on Flow Patterns in the Ascending Aorta ," *J. Biomech. Eng.*, vol. 125, no. 3, pp. 347–354, Jun. 2003, doi: 10.1115/1.1574332.

[90]   J. Lantz, J. Renner, and M. Karlsson, "Wall shear stress in a subject specific human aorta — Influence of fluid-structure interaction," *Int. J. Appl. Mech.*, vol. 03, no. 04, pp. 759–778, Dec. 2011, doi: 10.1142/S1758825111001226.

[91]   A. Leuprecht, S. Kozerke, and P. Boesiger, "Blood flow in the human ascending aorta : a combined MRI and CFD study," pp. 387–404, 2003.

[92]   J. Renner and G. Roland, "A Method for Subject Specific Estimation of Aortic Wall Shear Stress," vol. 6, no. 3, pp. 49–57, 2009.

[93]   F. P. P. Tan, A. Borghi, R. H. Mohiaddin, N. B. Wood, S. Thom, and X. Y. Xu, "Analysis of flow patterns in a patient-specific thoracic aortic aneurysm model," *Comput. Struct.*, vol. 87, no. 11–12, pp. 680–690, 2009, doi: 10.1016/j.compstruc.2008.09.007.

[94]   C-Y. Wen, En, A-S. Yang, L-Y. Tseng, and J-W. Chai, "Investigation of Pulsatile Flowfield in Healthy Thoracic Aorta Models," vol. 38, no. 2, pp. 391–402, 2010, doi: 10.1007/s10439-009-9835-6.

[95]   H. Isoda *et al.*, "Comparison of hemodynamics of intracranial aneurysms between MR fluid dynamics using 3D cine phase-contrast MRI and MR-based computational fluid dynamics," *Neuroradiology*, vol. 52, no. 10, pp. 913–920, 2010, doi: 10.1007/s00234-009-0634-4.

[96]   M. A. H. Mohd Adib, S. Ii, Y. Watanabe, and S. Wada, "Minimizing the blood velocity differences between phase-contrast magnetic resonance imaging and computational fluid dynamics simulation in cerebral arteries and aneurysms," *Med. Biol. Eng. Comput.*, vol. 55, no. 9, pp. 1605–1619, 2017, doi: 10.1007/s11517-017-1617-y.

[97]   S. Ii, M. A. H. M. Adib, Y. Watanabe, and S. Wada, "Physically consistent data assimilation method based on feedback control for patient-specific blood flow analysis," *Int. j. numer. method. biomed. eng.*, vol. 34, no. 1, pp. 1–20, 2018, doi: 10.1002/cnm.2910.